Materials Horizons

Tough and Circular Glass Fiber Composites via Tailored Dynamic Boronic Ester Interface

Journal:	*Materials Horizons*
Manuscript ID	MH-COM-10-2024-001452
Article Type:	Communication
Date Submitted by the Author:	17-Oct-2024

Complete List of Authors:	Mahappu Koralalage, Menisha; Oak Ridge National Laboratory, Chemical Sciences Division Rahman, Anisur; Oak Ridge National Laboratory, Chemical Sciences Division Yang, Guang; Oak Ridge National Laboratory, Chemical Sciences Division Gainaru, Catalin ; Oak Ridge National Laboratory, Chemical Sciences Division Demchuk, Zoriana; Oak Ridge National Laboratory, Chemical Sciences Division Bowland, Christopher; Oak Ridge National Laboratory, Chemical Sciences Division Meyer, Harry; Oak Ridge National Laboratory, Chemical Sciences Division Ghezawi, Natasha; The University of Tennessee Knoxville, Bredesen Center for Interdisciplinary Research and Education Saito, Tomonori; Oak Ridge National Laboratory, Chemical Sciences Division; The University of Tennessee Knoxville, Bredesen Center for Interdisciplinary Research and Education

New Concepts

Fiber reinforced polymer (FRP) composites are crucial lightweight structural materials, with their properties dictated by the fiber-matrix interface as well as the strengths of the fibers and matrix. A common method to strengthen the fiber-matrix interface is by applying sizing to the fiber surface. Here, we have designed a vitrimer that forms dynamic covalent bonds with pristine glass fiber (GF) surface, eliminating the need for sizing treatments, mitigating delamination issues, and enabling GFRPs with closed-loop circularity. The tailored interface of the glass fiber reinforced vitrimer (GFRV) composite significantly enhances mechanical properties and fiber-matrix interfacial adhesion, while enabling facile recyclability of both glass fibers and matrix. The dynamic covalent bonding within the matrix and the interface significantly increases in-plane shear toughness, offers fast thermoformability, and ensures exceptional adhesion to dissimilar surfaces. Given that GFRPs dominate the market, this strategy is particularly suitable for fibers with abundant hydroxyl groups, paving the way for sustainable, recyclable, and multifunctional structural materials as a viable alternative to non-recyclable thermoset GFRPs.

Tough and Circular Glass Fiber Composites via Tailored Dynamic Boronic Ester Interface

Menisha S. Karunarathna[1], Md Anisur Rahman[1], Guang Yang[1], Catalin Gainaru[1], Zoriana Demchuck[1], Christopher C. Bowland[1], Harry M Meyer III[1], Natasha Ghezawi[2], Tomonori Saito[1, 2]**

[1]Chemical Sciences Division, Oak Ridge National Laboratory, Oak Ridge, TN 37831, USA

[2]Bredesen Center for Interdisciplinary Research and Education, University of Tennessee Knoxville, Knoxville, TN 37966, USA

Keywords: Glass fiber reinforced composites, dynamic bonds, closed-loop circularity, vitrimers, dynamic interface

Abstract

Glass fiber reinforced polymer (GFRP) composites are valued for their strength and cost-effectiveness. However, traditional GFRPs often face challenges for end-of-life recycling due to their non-depolymerizable thermoset matrices, and long-term performance due to inadequate interfacial adhesion, which can lead to fiber-matrix delamination. Here, we have designed dynamic fiber-matrix interfaces to allow tough and closed-loop recyclable GFRPs by utilizing a vitrimer, derived from upcycled polystyrene-b-poly(ethylene-co-butylene)-b-polystyrene (SEBS) with boronic ester (S-Bpin) and amine-based diol crosslinker. The boronic ester groups in S-Bpin form dynamic covalent bonds with the naturally present hydroxyl groups on the unsized GF surface, that eliminates the need for fiber sizing and enables facile closed-loop recyclability of both the fibers and the vitrimer matrix. The resulting strong fiber-matrix interface, depicted by the Raman mapping, leads to a 552% increase in-plane shear toughness (6.2 ± 0.3 MJ/m^{-3}) and 27% ultimate tensile strength (361±89.2 MPa) compared to those of the conventional epoxy-based matrix (0.95 ± 0.05 MJ/m^{-3} and 264±59.7 MPa, respectively). The network rearrangement through dynamic boronic ester exchange enables fast thermoformability and repairability of micro-cracks at elevated temperatures. Additionally, both matrix and composite demonstrate strong adhesion to various surfaces including steel and glasses exhibiting $\geq$ 6 MPa lap shear strength, that expands their suitability for diverse industrial applications. The readily created dynamic interface between boronic ester functionalized vitrimer and neat GFs presents a promising strategy for developing

closed-loop recyclable, multifunctional structural materials, offering a sustainable alternative to non-recyclable thermoset GFRPs and contributes to a circular economy in composite materials.

Introduction

Fiber-reinforced polymer composites (FRPs), with their exceptional strength to weight ratios, are widely favored in various industries. Glass fiber reinforced polymer (GFRP) composites, in particular, dominate ~95% of the market with an annual growth rate of 5.6% due to their excellent mechanical properties, durability, and cost-effectiveness. GFRP composites are increasingly in demand for lightweight, high-strength applications in the automotive, aerospace, construction, and wind energy sectors. [1]

The matrix of FRPs can be either thermoplastic or thermoset, each offering unique properties and advantages. Thermoset matrices such as epoxy, unsaturated polyester, and vinyl ester are traditionally used in GFRPs due to their high strength and resistance to temperature and impact. However, they are not easily recyclable, making their end-of-life management challenging. Significant waste generation is particularly notable from wind turbine blades, which constitute 62 wt% of GFRPs.[2] By 2025, wind turbines are estimated to produce 66,000 tons/year of waste, leading to stricter regulations on composite disposal.[3] The poor recyclability, along with the energy-intensive nature of producing glass fibers (GFs) (requiring approximately 89-187 MJ/kg) and matrices, has prompted industries to reconsider the use of non-recyclable thermoset composites.[2] Existing recycling methods such as mechanical grinding and pyrolysis can cause significant loss of fiber strength up to 80%, as well as significant energy and greenhouse gas (GHG) emissions. Therefore, it is imperative to develop a closed-loop, low energy/carbon recycling method that preserves both fiber and matrix integrity.

Another prevailing challenge with traditional GFRP composites lies in inadequate adhesion between the matrix and the fiber surface. The anisotropic nature of GFRP composites frequently leads to damages such as delamination, burrs, fiber pull-outs, matrix smearing, and tearing.[4, 5] These issues predominantly stem from the poor interfacial adhesion between the fibers and the matrix.[6] Therefore, enhancing the interfacial adhesion between the fiber and the matrix is crucial for producing high-strength composites. Various methods for modifying GFs, such as alkali treatment, acetylation, grafting, and surface treatments like electroplating and plasma treatment, have been widely employed to improve interfacial adhesion.[7-9] However, these approaches often entail compromises in production cost, energy input, manufacturing complexity, and time. Hence, our primary goal is to develop a simple yet effective method to enhance the fiber-matrix interface without increasing manufacturing complexity, which we achieve by creating a boronic ester interface between the unmodified fiber surface and the matrix.

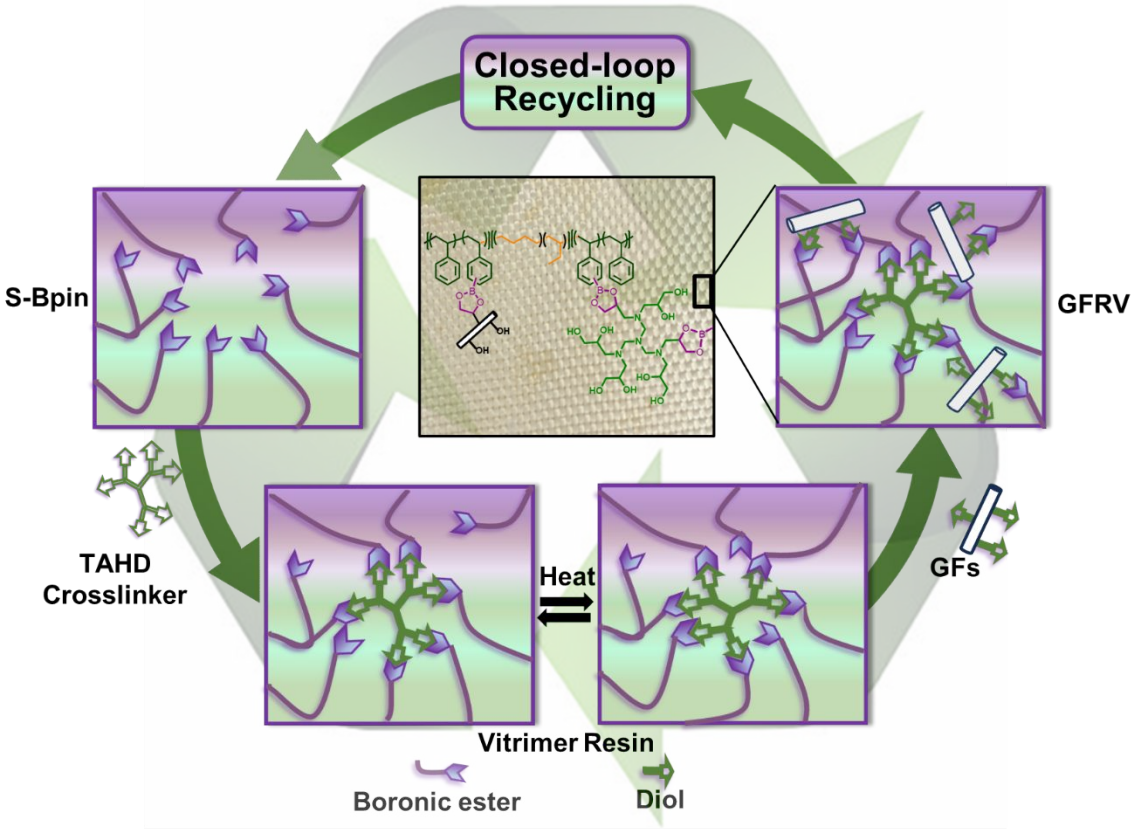

Figure 1. Closed-loop circularity of dynamic functionalized GFRV Composite.

To tackle these challenges, we have developed a closed-loop recyclable GFRP composite by using a commodity thermoplastic polymer with tailored covalent dynamic bonds as the matrix, which establishes a strong interface between the fiber surface and the matrix. The presence of covalent dynamic bonds such as boronic esters,[10-12] imine,[6, 13] vinylogous-urethane,[14] transesterifications,[15] disulfides,[16, 17] and urea[18] in vitrimers allows to rearrange with heat as well as other stimuli, including light or pH, offering attractive features like recyclability, malleability, shape memory, and self-healing.[19] Although the FRP composites with vitrimer matrices have been previously reported, developing a vitrimer matrix that ensures strong fiber matrix interfacial adhesion remains a significant challenge. Previous efforts have predominantly concentrated on modifying fibers prior to establishing dynamic bonds with the matrix.[16, 20, 21] In contrast, our approach in this study focuses on facilitating dynamic chemistry between the unmodified GF surface and the matrix to enable tough, closed loop recyclable glass fiber reinforced vitrimer (GFRV) composites. We designed to incorporate a boronic ester-modified upcycled thermoplastic elastomer, a multi-diol crosslinker, and neat GFs for achieving exceptional interfacial adhesion and recyclability. GFs naturally possess silanol groups on their surface, and we hypothesized that the boronic ester groups on the vitrimer matrix could dynamically crosslink with the free hydroxyl groups on neat GF surface, without sizing. (Figure 1). The excellent interface was manifested by the enhanced mechanical and interface properties by tensile experiment and Raman mapping. The reversible nature of the boronic ester exchange reaction on the crosslinks enables thermoformability, matrix

repair, closed-loop recycling, and superior interfacial interactions with fibers. The prepared GFRV composites exhibit significantly enhanced interfacial adhesion and toughness, as demonstrated in unidirectional and 45-degree tensile properties.

Additionally, a comprehensive "cradle to gate" life cycle analysis (LCA) exhibits a significantly low environmental impact and low cumulative energy demand for the GFRV compared to commercial GFRP, which provides a sustainable alternative. Furthermore, the tailored vitrimer and GFRV composites exhibit excellent adhesion to various surfaces including glass, aluminum, and steel. The GFRV composites, in particular, stand out as adhesive-free composites when attaching dissimilar materials, making them suitable for facile processing with dissimilar surfaces, especially in the automotive industry.

This study presents a straightforward approach to enhance GFRP recyclability and mechanical properties by utilizing dynamic chemistry between polymer matrix and unmodified GF surface. Due to no need for fiber sizing treatment, this approach provides a facile design of composite with a tailored dynamic bonding at fiber-matrix interface. These findings offer valuable insights into the design of circular GFRPs, leading to the development of multifunctional and sustainable structural materials for industries such as automotive, wind turbines, and construction.

Results and Discussion

Tailored S-Bpin Polymers with the Multi Diol-Crosslinkers

A commodity thermoplastic polymer, SEBS, was selected to be upcycled to vitrimer, which forms GFRV with the tailored interface. The microphase-separated SEBS triblock polymer comprises soft ethylene-butylene segments that dissipate energy and hard styrene blocks. The hard styrene blocks were borylated (S-Bpin) and crosslinked with multi-diols to prepare a vitrimer, following a previously reported method.[12] To control the thermomechanical properties, the boronic ester functionality of the S-Bpin was tailored by changing the reaction time of the boronic ester grafting. ^{1}H NMR determined the functionality of the S-Bpin as 10, 38, and 65% after reacting 2, 4, and 6 h, respectively (Figure S1). The dynamic mechanical analysis shows that the glass transition temperatures (T_g) of the borylated polystyrene block in S-Bpin increased gradually with the increased functionality, while the T_g of ethylene butylene containing midblock remains constant (-40 °C) (Figure S2). The highest boronic ester functionality of 65% exhibited the highest T_g of 160 °C, followed by T_g values of 130 °C and 108 °C, with 38% and 10% boronic ester functionality, respectively. Considering the matrix processing, medium T_g (130 °C) provides facile fiber-matrix thermal processing by better penetration throughout fibers in addition to sufficient thermal stability for most of the applications. The rubbery plateau of the functionalized S-Bpin in the storage modulus increases with more boronic ester grafting due to increased stiffness. We performed the tensile testing for each functionalized S-Bpin to evaluate the mechanical properties. As shown in Figure S3, the 38% functionalized S-Bpin exhibits the highest mechanical properties as 19.0 MPa tensile strength and 652 % elongation, compared to that of 10% functionalized S-Bpin (14.4 MPa, 627%) and 68% functionalized S-Bpin (13.9 MPa, 575%). The increased boronic ester

functionalization likely increases the rigidity of the overall polymer as seen in the increase of T_g of borylated polystyrene block, resulting in higher tensile strength than that of SEBS (12.1 MPa, 596%). The balance of the increased rigidity and elasticity resulted in the highest tensile strength and elongation for medium (38%) functionalized S-Bpin.

Subsequently, the boronic ester-based vitrimer was prepared by crosslinking S-Bpin with a multi-diol TAHD (Tris aminohexadiol) crosslinker (Figure 2A). The TAHD crosslinker comprises six diol arms, which can readily create a crosslinked polymeric network with boronic esters on S-Bpin. The S-Bpin in THF solution was mixed with the TAHD multi-diol crosslinker in a small amount of DMF. Based on the boronic ester functionalization of 65, 38, and 10 %, the constant amount of TAHD crosslinker was used as 5 mol% equivalents of grafted boronic esters to crosslink S-Bpin. S-Bpin−TAHD crosslinker mixture was air-dried at room temperature, followed by drying under reduced pressure at 120 °C. The dried TAHD S-Bpin mixtures were hot pressed at 180 °C for 1 h under ~1-ton pressure to cure the films fully (Figure 2H). The detailed synthesis of the vitrimer is described in the supporting information. The presence of crosslinking was confirmed by FTIR (Figure S4), where sharp peaks appeared at 1355 cm^{-1} and 1140 cm^{-1} corresponding to the B-O bond, and broad -OH group of the crosslinker disappeared at 3500 cm^{-1}. The DMA storage modulus curve of the uncrosslinked S-Bpin resin (Figure S2) shows no plateau, instead displaying a continuous slope, similar to thermoplastic SEBS. After crosslinking (Figure 2B), while the second rubbery plateau is not prominent in the S-Bpin 10%+TAHD sample due to low crosslink density, it becomes distinct in the higher crosslinked samples (65% and 38% S-Bpin+TAHD). This second rubbery plateau indicates additional stored elastic energy beyond the contribution of the styrene and the remaining blocks. Its appearance further reinforces the successful crosslinking in the S-Bpin+TAHD. The effective crosslink density of S-Bpin+TAHD can be determined using the rubber elasticity equation ($E = 3RTv$). The crosslink density per unit volume was estimated from the 2nd rubbery plateau over 200 ºC, that decreased from the highest to the lowest functionalized S-Bpin+TAHD: 251.0 mol m^{-3}, 198 mol m^{-3}, and 179 mol m^{-3} for the 65%, 38%, and 10 % S-Bpin+TAHD, respectively. The crosslinking of S-Bpin + TAHD also results in increased T_g compared to uncrosslinked S-Bpins due to requiring higher energy for the molecular segments to move in the crosslinked structure. As presented in Figure 2C, the S-Bpin 65% +TAHD, S-Bpin 38%+TAHD, S-Bpin 10%+TAHD exhibit T_g of 168, 156, 111°C, respectively with 8, 26, 3-degree increases, compared to their uncrosslinked S-Bpin, respectively (Figure 2C and Figure S2). The relatively lower T_g in the medium crosslinked S-Bpin 38%+TAHD showed better thermal processing and good flowability than the high and lower end of the functionalities.

The tensile properties of the crosslinked S-Bpins were evaluated. The medium functionalized S-Bpin 38%+TAHD outperformed the S-Bpin 65% +TAHD and S-Bpin 10%+TAHD, giving 32.3 MPa ultimate tensile strength (Figure 2D). As discussed above, S-Bpin 65% +TAHD exhibited the highest crosslink density. When the crosslink density is higher, the molecular movements are limited, which imparts a brittle nature upon applying stress. Therefore, S-Bpin 65% +TAHD show limited elongation, while S-Bpin10%+TAHD with very low crosslink density is not enough to make a protruding change in the mechanical properties, especially in tensile strength. Concurrently the medium functionalized S-Bpin 38%+TAHD exhibited higher toughness (the area underneath

the tensile stress-strain curve) of 72.6 MJ/m^3 compared to the S-Bpin 65% +TAHD and S-Bpin 10% +TAHD as 50.7 and 50.8 MJ/m^3 respectively (Figure 2E). Having higher toughness is also essential in the film's capacity to resist the formation of cracks near defects in the film due to stress accumulation.

To optimize the amount of the crosslinker for a high mechanical property with facile processability, we investigated different percentages (5, 10, 20 mol%) of the multidiol TAHD crosslinker with medium functionalized S-Bpin. The S-Bpin 38%+5 mol% TAHD exhibited the highest mechanical properties of a 28.2 % increase in tensile strength and a 43.2 % elongation increase compared to those of 20% TAHD crosslinker (Figure 2F). As discussed above, the higher crosslink density (e.g., S-Bpin 65%+TAHD) does not improve the mechanical properties. Thus, the lowest percentage of the crosslinker with medium functionalized S-Bpin 38% exhibited well-balanced thermal and mechanical properties with excellent toughness, providing greater resistance to fracture upon stress. Therefore, S-Bpin 38%+5mol% TAHD was selected for further analysis and denoted as S-Bpin+TAHD throughout the rest of the manuscript.

The resistance for the solvents was analyzed with the S-Bpin+TAHD. As shown in Figure 2I, S-Bpin+TAHD films were immersed in different solvents such as dichloromethane (DCM), THF, dimethylformamide (DMF), methanol (MeOH), hexane, and deionized water for 24 h at room temperature, and the solubility was monitored. The crosslinked samples of S-Bpin+TAHD did not dissolve in any solvents, although some degree of swelling was observed in DCM, and THF, exhibiting resistance to a wide range of solvents due to the crosslinked structure and the hydrophobic nature of the S-Bpin polymer.

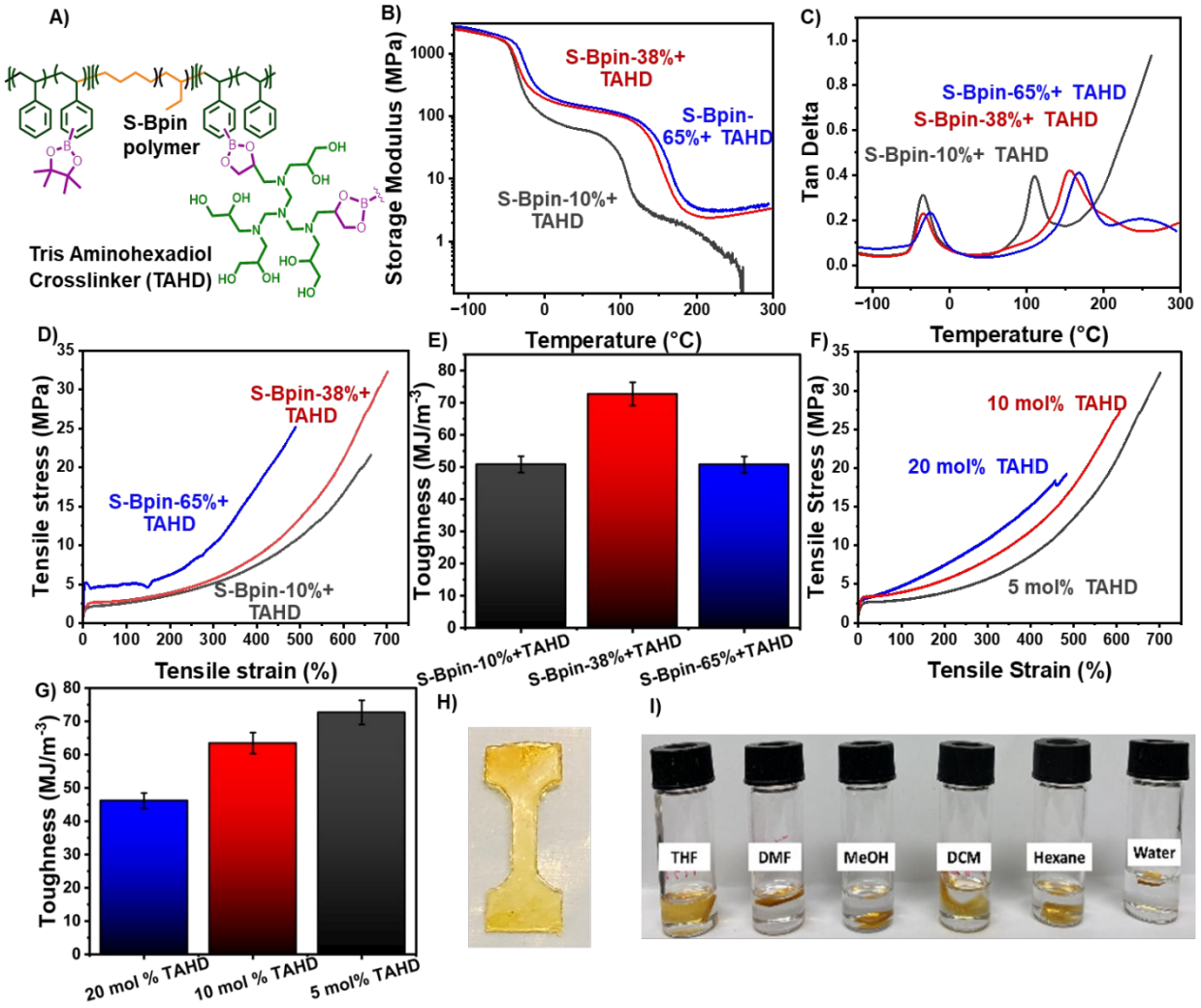

Figure 2. Composition of the new vitrimer and the tailored mechanical and thermal properties. A) Schematic illustration of multi-diol crosslinked vitrimer from modified SEBS (S-Bpin) and TAHD crosslinker; B) The dynamic mechanical analysis (DMA) of functionality tailored S-Bpin with 5 mol% TAHD, exhibiting storage modulus as a function of temperature; C) Tan delta versus temperature for functionality tailored S-Bpin with 5 mol% TAHD; D) Uniaxial tensile stress-strain curves of functionality tailored S-Bpin with 5 mol% TAHD until failure E) Toughness values from the tensile experiment, D. The error bars indicate SDs from triplicate measurements; F) tensile stress-strain curves of S-Bpin 38% with varied crosslinker percentages; G) Toughness values from the tensile experiment, F; H) Dog bone sample of the S-Bpin+TAHD; I) The solvent resistance test of S-Bpin+TAHD in different solvents at room temperature for 24 hrs.

Design and mechanical properties of GFRV

The GFRV composites were prepared by impregnating the woven S-Glass fibers (fabric hexcel hex force fiberglass s-glass plain weave style) in a solution of THF and S-Bpin+TAHD. The 3-ply composites were prepared by partial curing at 120 °C, followed by hot pressing at 180 °C for 45 minutes. The schematic representation of fiber preparation is illustrated in Figure 3A, and the detailed procedure is given in the supporting information. The matrix percentage was confirmed as ~30 wt% by the TGA analysis (Figure 3B). The S-Bpin polymer can form strong dynamic covalent bonds with the hydroxyls on silica surfaces via either a monodentate or a bidentate fashion, where the monodentate binding was estimated to be 72 kJ/mol.[12] With the naturally abundant free -OH groups on the GF surface, the S-Bpin+TAHD vitrimer can exchange -OH groups on the fiber, improving fiber-matrix adhesion. To assess the heterogeneity/microstructure characterizations of the fiber-matrix interface and the interfacial interaction, we conducted Raman mapping with clustering analysis on the cross-section of unsized-GF_S-Bpin and unsized GF_SEBS composites. These composites were synthesized without any crosslinker. Figure 3C and 3D show the Raman mapping spectra of GF_S-Bpin and GF_SEBS composites, respectively, which can be classified into five clusters, color-coded with five different colors. In both samples, a brown coded region was observed at the interface between the GF and the polymer region, allowing us to directly compare the interfacial chemistry between the two samples. Figure 3E shows that the GF_S-Bpin has a distinct peak centered at 1602 cm^{-1}, that is not present on the GF_SEBS surface. This peak corresponds to the boronic acid structure, stemming from the boronic ester moieties in S-Bpin. The peak centered at 2222 cm^{-1} may result from the asymmetric N-C-O stretching mode which should result from the B-O-C-N moity.[22] Furthermore, a careful analysis of the range 2500-3500 cm^{-1} indicates that the interface between GF_S-Bpin shows a prominent 3166 cm^{-1} peak (O-H stretching) that is absent in the GF_SEBS sample, probably due to the boronic ester groups generated as a result of the dynamic bond exchange with the hydroxyl groups on GF surface. These findings indicate that the unsized GF can form a strong interface with the S-Bpin via dynamic covalent bonding.

The mechanical properties of the prepared GFRVs were evaluated using unidirectional tensile testing and compared to GFRP composites made from conventional epoxy (control-1) and unmodified SEBS (control-2) under identical conditions. While epoxy GFRP composites are widely used, comparing mechanical data can be challenging due to variations in factors like fiber type, orientation, ply count, fiber volume, and strain rate.[23-25] Therefore, we compared a traditional epoxy-based composite prepared under the same processing conditions for consistency. Notably, the ultimate tensile strength and toughness of GFRV composites (Figure 3F and 3G) reached 361±89.2 MPa and 22.8 $\pm$ 1.4 MJ/m^{-3}, respectively, which are 27% and 85% higher than that of the conventional epoxy-based GFRP (control-1). Conventional epoxy shows limited flexibility; thus, the further movement of the glass fiber fractures the epoxy matrix, resulting in lower elongation and toughness. Unlike the GFRV composites, epoxy groups have minimal to no covalently bound functional groups with the GF surface. The GFRV composites exhibited a 30% and 79% increase in ultimate tensile strength and toughness compared to control 2 with pristine SEBS matrix without boronic ester functionalization or crosslinker. This result also reinforces that

fiber-matrix adhesion plays a vital role in providing higher mechanical properties as the SEBS, without any exchangeable diol groups, cannot maintain good bonding between the fiber and the matrix. To evaluate the interfacial adhesion between the fiber and matrix, the uniaxial tensile strength of 45-degree fiber-oriented GFRVs was tested. The resulting tensile stress and toughness data (Figure 3H and 3I) evidently designate a significant increase of 500% and 693 % in tensile stress and toughness than control 2 composites with SEBS matrix. Although the conventional epoxy GFRP sample reported a 25% higher tensile stress than that of the GFRV composites, the GFRP composites snapped immediately, resulting in lower elongation. The GFRV exhibited excellent in-plane shear toughness with a 552% increase compared to the epoxy control. Although the rigidity of the epoxy matrix withstands higher stress while being stretched before breaking, its inability to maintain flexibility resulted in a very low strain, thus significantly reducing its toughness. As shown in Figure 3J, the illustration of the specimens after the tensile testing clearly indicates significant damage propagation in epoxy GFRP and minimum damage in the GFRV. Due to the limited flexibility of epoxy matrices over the substrates, matrix fracture often happens, causing more localized damage. In contrast, the GFRV composite shows minimum damage to the fibers as the matrix has better flexibility and, more importantly, good interfacial adhesion. This is crucial in applications, where the use of rigid matrix is limited due to the need for a certain degree of elongation or deformation.

As illustrated in Figure 3F, the epoxy and the SEBS tensile curves show early slippage before reaching ultimate strength due to transverse microcracking.[26] When the composite reaches a certain stress level, the matrix starts to crack away from the fiber alignment due to poor interfacial adhesion. At this stage, the breakdown of the laminate has already begun, even though the composite has not completely failed. Additionally, these microcracks can absorb water, increase weight, and compromise the effectiveness of the fiber sizing agent (while GF in this study does not have sizing) and the matrix, leading to a loss of the ultimate properties of the entire composite. In contrast, GFRV does not exhibit early slippage, indicating better lamination between the fiber and the matrix due to enhanced interfacial adhesion.

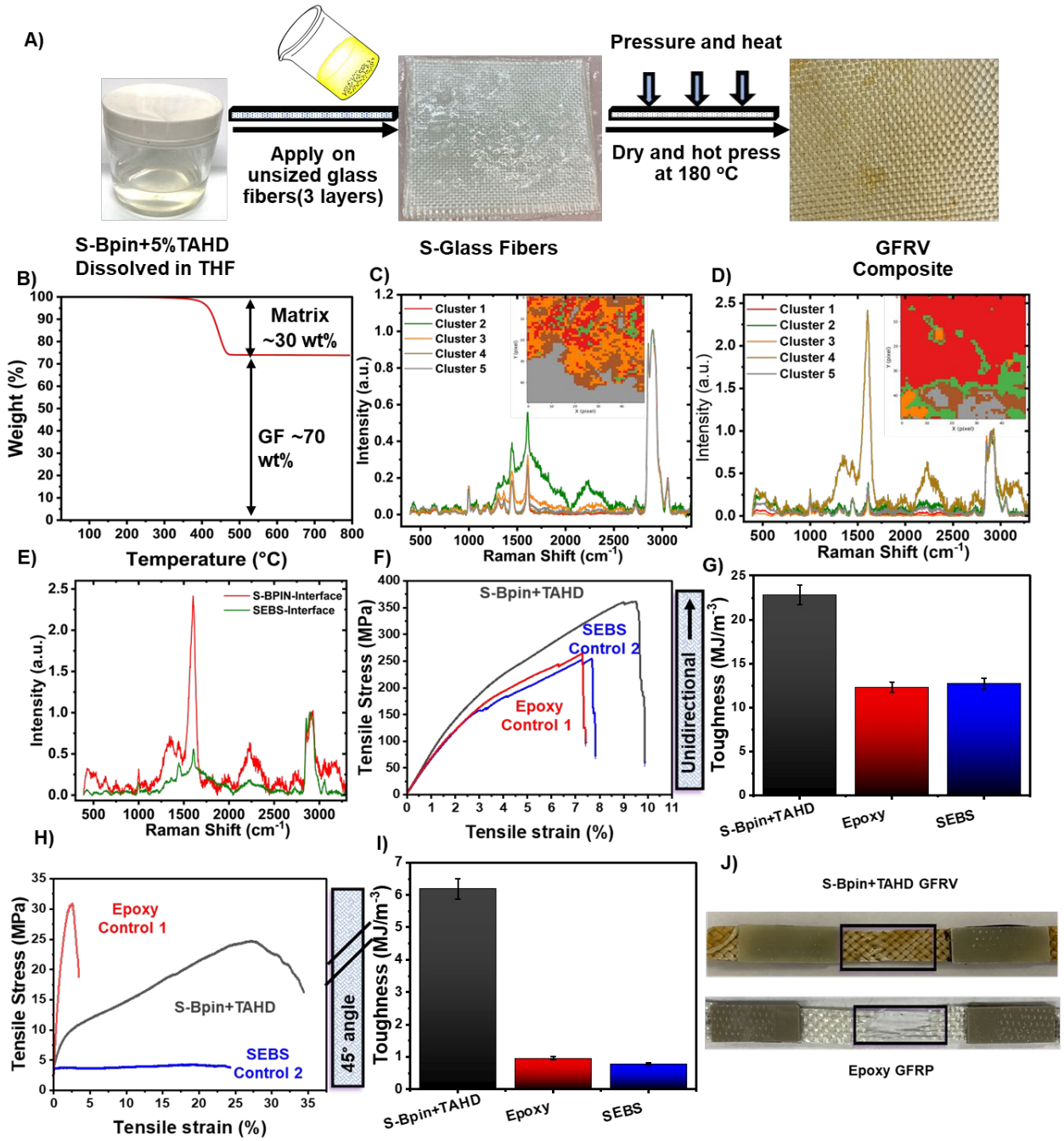

Figure 3. Design and mechanical properties of GFRV. A) Schematic representation for the fabrication of GFRV; B) TGA of GFRV composite exhibiting the amount of polymer content; C) The K-cluster centroid spectra were taken from different color-coded regions corresponding to K-means cluster analysis (represented in the inset) of the Raman mapping of the unsized GF-SEBS sample with Raman mapping scaling 2902 cm^{-1} peak intensity shown in Figure S5; D) The K-cluster centroid spectra for different color-coded regions corresponding to the K-means cluster analysis of unsized GF-S-Bpin sample, shown in the inset (Raman mapping scaling of 2902 cm^{-1} peak intensity shown in Figure S6); E) Comparison of the interfacial Raman spectra between sized GF-SEBS and unsized GF-S-Bpin; F) Unidirectional tensile stress-strain curves of the GFRV

composites with controls; G) Toughness comparison of GFRV composites with the controls; H) Fiber-matrix-in plane shear stress analysis via 45° angle tensile stress-strain test; I) In-plane shear toughness comparison with the controls; F); J) Illustration of the damage localization of the conventional epoxy and the GFRV composite samples.

The Viscoelastic Properties Analysis

A thermally processable matrix for FRP composites requires a matrix to have sufficient flow properties. We employed rheological analysis to assess the viscoelastic behavior of the S-Bpin+TAHD system. The stress relaxation tests have been performed using a constant strain of 2% to access shear modulus decays at temperatures between 182 °C and 232 °C and in a dynamic range covering 0.1 – 10,000 s. Figure 4A presents the stress relaxation results obtained for the S-Bpin+TAHD crosslinked sample covering 5 decades in time *t*. The curves have been normalized vertically to overlap at $t = 0.1$ s to a common "initial" shear modulus value $G(i) = 1$. The semi-logarithmic representation of the data curves allows for the identification of two contributions, one emerging as a linear decay at relatively short times as best recognized at the lowest investigated temperature (182 °C), and a sigmoidal one as the fingerprint of a slow relaxation mode. Since the curve probed at 232 °C decays almost to zero in the available experimental window, this slow relaxation feature can be safely assigned to the terminal flow. As recently demonstrated, this bimodal shear response appears to be a hallmark of crosslinked vitrimers.[27] To quantify the temperature evolution of the probed shear dynamics, we used two methods proposed in the related literature: i) The first one relies on plotting the normalized shear relaxation curves on a linear time scale (Figure S7), then simply collecting the time scales corresponding to a decay of $G(t)/G(i)$ by a factor of 1/e for each temperature. The "1/e" method is the conventional approach for analyzing stress relaxation of vitrimers, despite assuming a monomodal and exponential terminal response. The extracted dynamic parameters depend on the initial normalization conditions.[28] For comparison with various vitrimer studies, we used this method to extract corresponding time scales and included them in Figure 4A. A second method, recently applied to vitrimers, uses shift factors determined from time-temperature superposition of the shear response. This classical approach for polymers allows analysis of individual relaxation processes, especially when the shear response is complex.[29] The application of this second method to the present material is presented in Figure. 4B. Here the curve probed at 232°C is used as a reference, while those probed at the other temperatures are shifted horizontally until the best overlap is achieved with respect to the fast process (I). Using the frequency shift factors corresponding to different temperatures, one can estimate the activation energy of this particular relaxation feature. As observed in Figure 4B, for the curves probed at 222 and 212°C, the same shift factors superimpose not only the fast, but also the slow dynamics (process II). At lower temperatures, additional shifts (indicated by the arrow) are needed to align the terminal relaxation, indicating different temperature dependencies for the two features. Process I's linear decay does not allow for characteristic time extraction. However, process II's curve at 232°C shows an inflection point on the log t scale. By using this inflection point's time scale and shift factors, one can estimate process II's characteristic times at other temperatures.

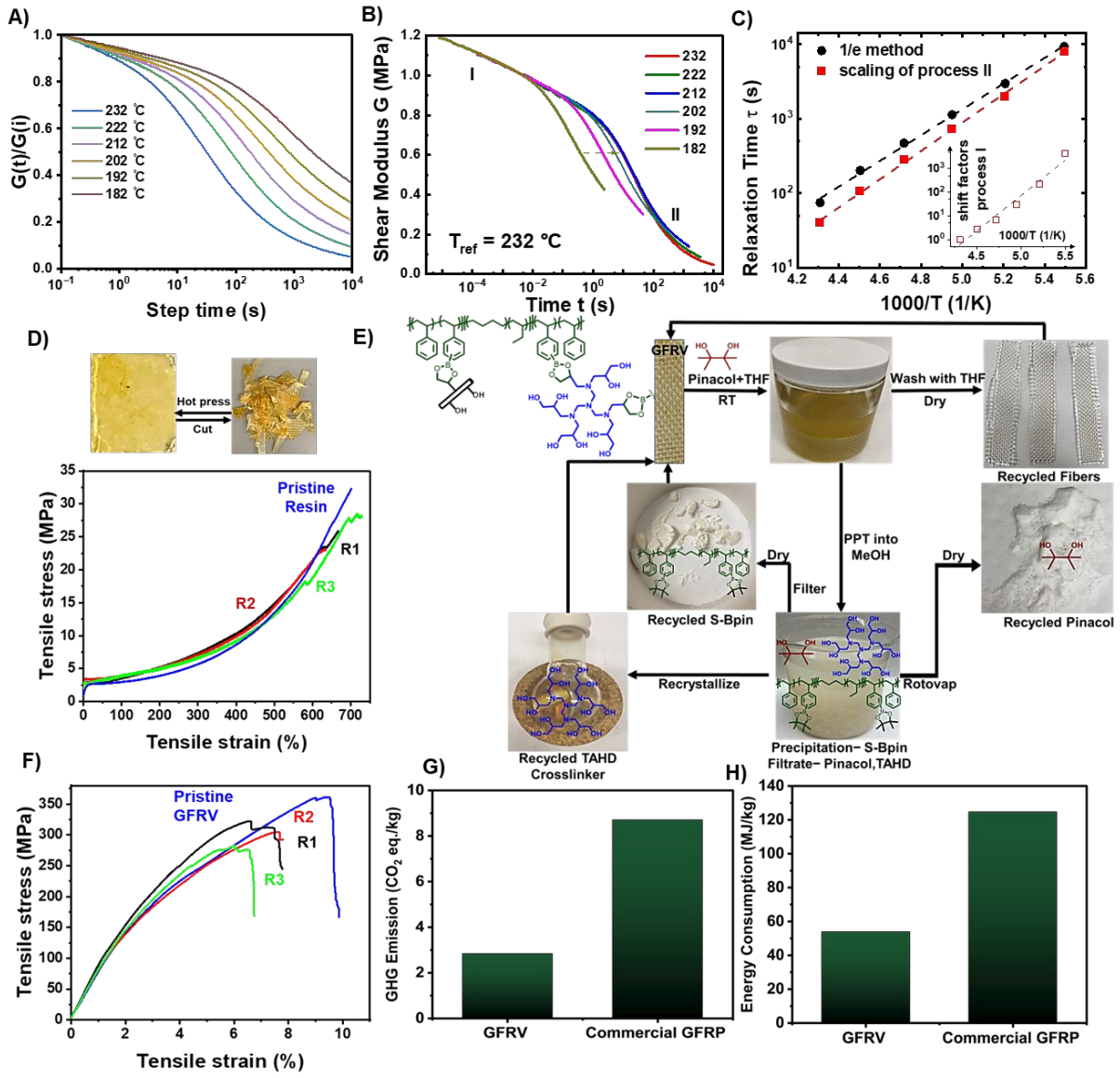

Figure 4. Thermomechanical behavior, recyclability and the environmental impact of GFRV composite. A) Normalized stress relaxation curves of S-Bpin+TAHD at a temperature range of 182 to 232°C with 10 °C intervals; B) Master plot of stress relaxation curves constructed for the reference temperature of 232°C; C) Relaxation time estimated using 1/e method (black dots) and time scales of process II extracted using an approach based on time-temperature superposition (red symbols). The inset represents process I shift factors with respect to the reference temperature of 232°C; D) Schematic representation of the thermal (re)processability of S-Bpin+TAHD and the tensile stress strain data; E) Illustration of the chemical recyclability of the GFRV composite; F) Uniaxial tensile properties of chemically recycled GFRV composite over 3 cycles; G) The bar chart to show the comparison of GHG emission between GFRV and commercial GFRP composites. Comparing 1 kg GFRV composite with 1 kg injection molded, polyamide based GFRP composite (Method: TRACI 2.1 V1.05 / US 2008 / Characterization / Excluding infrastructure

processes / Excluding long-term) H) The comparison of non-renewable energy consumption of GFRV and commercial GFRP composites.

Figure 4C presents the characteristic times extracted using both procedures. The black dots correspond to the "traditional" 1/e method and their interpolation with an Arrhenius law $\log \tau \propto \exp(E/RT)$ provides an activation energy of 33 kJ/mol. The red squares represent the time scales of process II extracted using an approach based on time-temperature superposition combined with the identification of the inflection point in the log t scale for the curve at the reference temperature. This method provides an activation energy for the terminal flow of 37 kJ/mol, hence 12% higher than the one estimated using the 1/e approach. Finally, since it was not possible to extract characteristic times for process I, the inset of Figure 4C presents its shift factors at the reference temperature of 232°C (for which the scaling factor is 1). The Arrhenius interpolation of these data provides a much higher activation energy, of about 130 kJ/mol. The energy barrier of the process I appears to be close to that of segmental relaxation of crosslinked S-Bpin blocks (11 kJ/mol) and smaller by a factor of two than that for the boronic ester exchange reaction (260 kJ/mol), which was reported in a recently investigated vitrimer.[27] Based on the corresponding shear modulus amplitude (in the 1 MPa range), the process I appears to be governed by the chain dynamics in the present material. As recently demonstrated, the temperature evolution of the latter can follow well that of segmental rearrangements in this high temperature regime.[28] On the other hand, much lower activation energy (37 kJ/mol) of process II, assigned in the present work to the terminal flow, indicates that the latter display a rather lower sensitivity to temperature variation. However, there are several examples in the literature, where terminal relaxation displays similar weak T variations. As demonstrated for a series of vitrimers with boronic ester functionalities, the activation energy for the terminal flow display values between 30 and 50 kJ/mol, hence similar with the one reported here for borylated multi-diol crosslinked polymer modified from SEBS.[30] Another recent study showed that polymer networks with both a pendant and telechelic architecture synthesized with mixed orthogonal dynamic bonds exhibit a much weaker temperature dependence of terminal viscoelastic times than the one displayed by the segmental dynamics.[31]

Thermal and Closed-loop Recyclability

As evidenced by the rheology analysis, the excellent flow behavior of S-Bpin+TAHD is directly beneficial for the thermal reprocessability. We assessed the thermal reprocessability by hot pressing the broken pieces of films under constant pressure for 15 minutes at 180 °C. Since the dynamic boronic esters can be rearranged with an associative mechanism, triggered by an external stimulus, a smooth film could be refabricated by simply hot pressing the broken pieces of previously used films. Figure 4D shows the mechanical properties of the thermally reprocessed films over 3 cycles. S-Bpin+TAHD vitrimer was able to keep the mechanical properties intact even after 3 consecutive thermal reprocess cycles. More importantly, these vitrimer composites can be chemically recycled in a closed-loop way. Closed-loop recyclability allows to reuse of the fibers and all the chemicals used in the process for the same or different applications. The closed-loop recycling provides a significant advantage compared to traditional thermoset GFRP composites like epoxy matrix composites. Based on the fact that the boronic esters can exchange bonds with diol groups, the S-Bpin+TAHD vitrimer matrix was dissolved in pinacol-THF solution. The diol

groups in pinacol can exchange the bonds with boronic esters, resulting in complete dissolution of the matrix. The S-Bpin polymer was recovered by precipitating into methanol with 96% recovery rate. The ^{1}H NMR of recovered S-Bpin is identical to the S-Bpin starting material, reassuring the purity of the recovered S-Bpin polymer (Figure S8). The recovered crosslinker and pure form of pinacol was obtained by rotary evaporating THF, followed by recrystallizing with water. ^{1}H NMR spectrum of recycled pinacol is consistent with its initial form, as demonstrated in Figure S9. The FTIR and ^{1}H NMR spectra of the recrystallized crosslinker were compared to the initial, and the peaks remained the same as the initial (Figure S10, S11). Hence, this chemical recycling process enables the recovery of all the chemicals in their pristine form.

The recovered S-Bpin was reused to make S-Bpin+TAHD vitrimer and the GFRV composite. Figure 4E illustrates the overall picture of the closed-loop recycled process. SEM images of recycled fibers confirm no deposition, showing a smooth surface similar to pristine fibers (Figure S12). These images support the successful closed-loop chemical recycling process, where fibers can be collected without apparent physical damage. The XPS data in Figure S13 indicate that the surface composition of recycled fibers closely resembles that of pristine fibers, as the recycled fibers are free of matrix after pinacol treatment. Elemental peaks in the recycled fibers show the same intensity as pristine unsized GFs, with the increased C peak possibly due to residual polymer.

Moreover, the prominent peak for oxygen in the full-scan XPS spectrum of pristine GFs indicates a high abundance of oxygen, and consequently, a greater fiber surface polarity. Oxygen (O) on the GF surface can exist as bridging oxygen (BO) and non-bridging oxygen (NBO). The detailed core-level spectra of the O1s region for pristine fibers reveal BO at approximately 533 eV and NBO at approximately 531 eV. The pristine fibers exhibit nearly equal amounts of BO and NBO, as evidenced by the fitted curves with peaks of similar heights (Figure S14).

Tensile testing of recycled composites (Figure 4G) shows maintained mechanical properties even after three complete recycling processes, with a slight decrease in toughness but no change in overall mechanical properties (within measurement error). The slight decline in toughness may be attributed to fiber misalignment during composite preparation, although the woven GFs were not visibly or mechanically damaged.

Life Cycle Analysis of GFRV

The closed-loop recycling of the polymer and fibers can substantially reduce the environmental impact of materials, leading to a significant reduction in embodied carbon. Our study conducted a comprehensive "cradle-to-gate" LCA for GFRV composites, which contain 70% GF reinforcement material. LCA, a methodology for evaluating environmental impacts at every stage of a product or process, was conducted across 10 distinct categories such as ozone depletion, global warming, and energy consumption of GFRV composites. This analysis was crucial in evaluating the potential sustainability of GFRV composites compared to commercial GFRPs in the market. Detailed findings of the LCA are presented in the SI.

Benefiting from an efficient recycling process, our GFRV composites exhibit significantly low GHG emissions, measuring 2.83 kg CO_2 eq. This emission value, derived from the key components involved in S-Bpin synthesis, was incorporated into the overall GHG emissions for 1 kg of GFRV,

as outlined in Tables S1 and S2. This represents a threefold reduction compared to commercial GFRP composites, which register at 8.7 kg CO_2 eq (Figure 4G, Table S1).

As shown in Figure S15, the modification of the original SEBS polymer into S-Bpin has a substantially lower environmental impact across various categories, including acidification, smog, eutrophication, carcinogenicity, ecotoxicity, respiratory effects, and fossil fuel depletion, compared to the synthesis of SEBS itself. Moreover, the environmental footprint of GFRV composites is reduced in comparison to commercial GFRPs (Figure S16). A comprehensive environmental impact assessment, considering GF production, S-Bpin synthesis, and energy consumption, is presented in Figure S17. Notably, the bar chart emphasizes that the greatest environmental burden arises from GF production across most categories, with the exception of ozone depletion. This finding underscores the critical importance to focus on fiber recycling rather than the production of new fibers for mitigating environmental impacts,

Overall, the GFRV composites display a very low cumulative energy demand (Figure S18). Our vitrimer composites demonstrate a significantly lower nonrenewable fossil energy demand, measuring 53.8 MJ/kg—nearly a twofold reduction compared to commercial GFRPs, which have a demand of 124.7 MJ/kg (Figure 4H, Table S6). (The calculation details can be found in Tables S3 and S4.) This result emphasizes the potential of our GFRV composites to be more sustainable and environmentally friendly materials of choice, offering a more sustainable alternative to conventional GFRPs.

Adhesion Properties on Dissimilar Materials and Thermoformability

As demonstrated by Raman mapping, S-Bpin maintains an excellent interface with GFs due to the presence of dynamic covalent bonds between boronic ester moieties and hydroxy groups on the fiber surface. Similar to the abundance of free Si-O-H groups on glass surfaces, aluminum and steel exhibit Al-O-H and Fe-O-H groups, respectively, within their oxidized layers. Consequently, the matrix alone demonstrates strong adhesion to hydroxyl-rich surfaces, including not only glass but also aluminum and steel. DFT calculations from our previous studies have shown that boronic moieties in S-Bpin polymer can form covalent bonds with hydroxyl groups present on these various surfaces, either through a monodentate or bidentate coordination mode.[12] We tested the adhesive properties of the following three samples including SEBS without dynamic bonds, SBpin_38%, and S-Bpin+TAHD, to glass, aluminum, and steel sheets with an overlapped surface area of 144 mm^2 (12 mm × 12 mm) following a modified version of ASTM D1002. SEBS is widely used as a hot-melt pressure-sensitive adhesive. As the modified SEBS with boronic ester moieties provides better capability to exchange bonds with hydroxyl-terminated surfaces, we hypothesized each surface to have better adhesion strength. As per Figure 5B, S-Bpin 38% adhesion strength was on par or slightly higher than SEBS for the three selected surfaces. Due to the crosslinked structure, S-Bpin+TAHD gives much higher adhesion strength with each surface than non-crosslinked S-Bpin 38%. Compared to SEBS, the lap shear adhesion strength of S-Bpin+TAHD on glass (5.9 ± 0.6 MPa) has been increased by 90%, while that on aluminum (3.7 ± 0.4 MPa) and steel (6.3 ± 0.5 MPa) increased by 67% and 117%, respectively. The significant increase in adhesion can be attributed to the likely occurrence of dynamic bond exchange between the matrix

and the surfaces. These results provide a good platform for a strong adhesive to use on multiple surfaces.

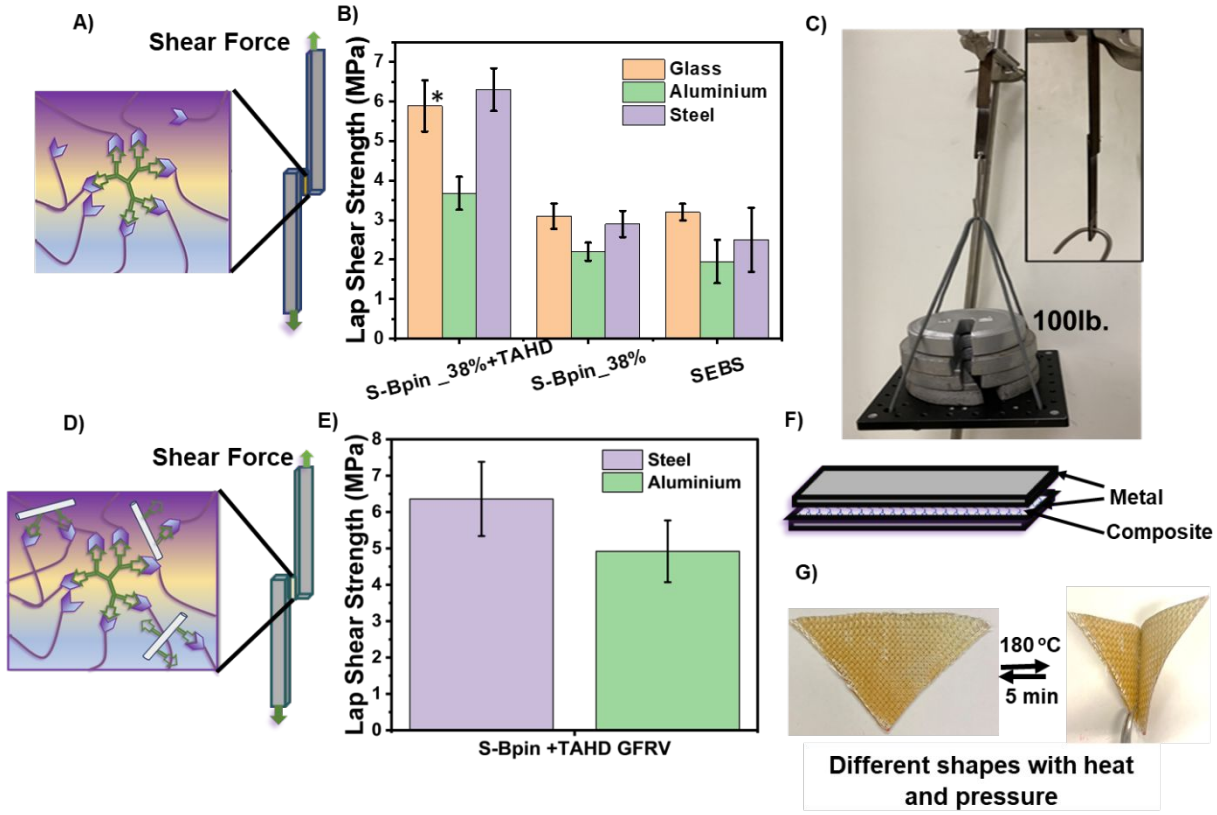

Figure 5. The adhesion and the thermoformability of GFRV Composites. A) Graphical representation of lap shear adhesion test for vitrimer films; B) Lap shear strength on different substrates using S-Bpin polymers (* Shows the substrate failure of glass, indicating that the adhesion strength can go higher than reported.); C) Demonstration of the adhesion strength with steel sheets; D) Graphical representation of lap shear adhesion test for GFRV composites; E) Lap shear adhesion strength analysis on metal substrates using GFRV composites; F) Schematic representation for metal-GFRP hybrid composites used in automotive industry; G) Thermoformability of GFRV composites.

The predominant method used in the fabrication of automotive components is sheet molding compounds (SMC) made of GFs impregnated with epoxy, unsaturated polyester, and vinyl ester matrix. However, the major impediment to using SMC in the automotive industry is the adhesion of dissimilar surfaces.[32, 33] The SMCs are likely to delaminate with metals because of the low adhesion strength of the metals and the composite surfaces. We demonstrate a strong adhesion and cohesive failure between the GFRVs and the metals directly without using any additional adhesives or primer. The composite was hot-pressed with the metals for 45 minutes, and the lap

shear strength was tested. The composites and the metal surfaces can maintain good adhesion bonding, resulting in ~6.3 MPa of lap-shear strength with steel and ~ 4.9 MPa with aluminum, which outperform the commercial bisphenol A epoxy-based adhesives (3.7-5.8 MPa).[34] Thus, the SMC or similar process can directly use the GFRV composite to attach dissimilar surfaces like metals with no additional surface preparation.

The GFRV composites exhibit thermoformability, despite being crosslinked. Dynamic boronic ester exchange allows these GFRV composites to be molded or deformed into different shapes just by applying heat and facilitates the repairability of micro-cracks within the composite matrix. As demonstrated in Figure 5G, the triangular composite sample was thermally deformed into a "V" shape at 180 °C. The deformed material maintained the V shape at room temperature until it was reformed into its initial triangular shape. The reshaping and remolding ability using dynamic boronic ester exchange offers an attractive option for many industries. The strategy reported here paves the way for an ongoing pursuit of recyclable, multitask structural materials.

Conclusions:

This study presents a facile strategy to prepare tough, recyclable GFRV, facilitated by dynamic covalent bonds between naturally occurring functional groups on the GF surface and a boronic ester-modified tough vitrimer matrix derived from a thermoplastic elastomer. The dynamic covalent bonds between fiber and the matrix allow enhanced mechanical properties and fiber-matrix interfacial adhesion without any surface treatment. The developed GFRVs exhibit a remarkable increase (552%) in-plane shear modulus of toughness compared to GFRPs from conventional epoxy-based matrices and reached 27% higher uniaxial ultimate tensile strength. The boronic ester bonds and amine-based diol crosslinkers allow for network rearrangement under specific temperatures, allowing fast thermoformability. Furthermore, the upcycled S-Bpin crosslinked polymer and GFRV composites demonstrate exceptional adhesion to various surfaces, including glass, aluminum, and steel, surpassing traditional structural bisphenol A epoxy-based adhesives. The GFRV composites exhibit a threefold lower greenhouse gas emission value and two-fold lower cumulative energy demand compared to those of commercial GFRP composites. This study reports a significant advancement in developing recyclable multifunctional structural materials, and the strategy offers a sustainable alternative to non-recyclable thermoset GFRPs, and promotes closed-loop recycling in composite materials.

EXPERIMENTAL SECTION

Materials

Polystyrene-*b*-poly(ethylene-*co*-butylene)-*b*-polystyrene (SEBS) (Mn = 118 kg/mol with Đ = 1.08; 30 mol % polystyrene repeating unit; 30 wt% polystyrene), 4,4′-di-tert-butyl bipyridine (dtbpy), chloro(1,5-cyclooctadiene)iridium(I) dimer ($[IrCl(COD)]_2$) and Tris(4-

hydroxyphenyl)methane triglycidyl ether were purchased from Sigma-Aldrich. Bis(pinacolato)diboron (B_2Pin_2) was purchased from oakwood chemicals. The crosslinker diglycerol, and Tris(2-aminoethyl)amine were purchased from Sigma-Aldrich and used without further purifications. The fabric hexcel hexforce fiberglass s-glass plain weave style 4533 f81 glass fiber (GF) was obtained from Composite Envisions, who sourced the materials from Hexcel. Anhydrous tetrahydrofuran (THF), ACS grade methanol, chloroform ($CHCl_3$), and dimethylformamide (DMF), ethyl acetate were purchased from Acros Organics. All the chemicals were used as received unless otherwise noted.

Characterization Methods

All ^{1}H NMR spectra were recorded on a Bruker Avance spectrometer operating at 400 MHz. Thermogravimetric analysis (TGA) data were recorded on a TGA Q50, TA Instrument over the range 20 to 800 °C, with a heating rate of 10°C min^{-1} under a flow of N_2 (40 mL min^{-1}). Fourier transform infrared (FTIR) spectra were obtained using an Agilent Technologies instrument operating over the range of 400–4000 cm^{-1} at ambient temperature using an ATR attachment.

Tensile Analysis

Tensile stress and strain of S-Bpin vitrimer samples were measured using an Instron 3343 universal testing system equipped with 1 KN sensor following the ASTM D1708 standard. A dog-bone tensile test piece die-cutting punch press was used to cut the dog-bone shape films with a width of 2.5 mm, a length of 7 mm, and an average thickness of 0.3 mm, which were tested at room temperature. The actual thicknesses, widths, and lengths were individually measured at several areas of each sample using a caliper. Samples were elongated at the rate of 1 mm s^{-1} till the break. Toughness was calculated from the area under the stress−strain curve. The mechanical properties data reported are average of at least three specimens run.

Tensile stress and strain of composite samples were measured using an Instron 3400 universal testing system equipped with 10 KN sensor following the ASTM D1708 standard. The composite samples were prepared by tabbing the two ends with plastic tabs to avoid fiber damage upon clamping. The samples were cut into rectangular samples using a wet saw with dimensions of 10 mm width, a length of 25 mm, and an average thickness of 0.5 mm. The actual thicknesses, widths, and lengths were individually measured at several areas of each sample using a caliper. Samples were elongated at the rate of 1 mm s^{-1} to observe the ultimate tensile strength.

Dynamic Mechanical Analysis (DMA)

Dynamic mechanical analysis (DMA) was measured by TA Instruments DMA 850 using a tension clamp. After hot-pressed at 180 °C, the films were cut into rectangular shapes. Each sample was tested in a temperature range from -120 °C to 300 °C at a rate of 3 °C min^{-1} with a frequency of 1 Hz and 15 μm amplitude.

The crosslink density of multidiol S-Bpin vitrimers was calculated from the plateau region of DMA plots. The crosslink density of multi-diol S-Bpin was determined using the rubber elasticity equation; $E = 3RTv$

Where v is the crosslink density, E is the storage modulus T temperature relating to E selected as 40 °C above the T_g and R is the universal gas constant (8.314 J^{-1} K^{-1} mol^{-1}).

Shear Rheology Measurements.

Rheological shear measurements were carried out by an ARES G2 rheometer (TA Instruments) using 8 mm plates with a parallel plate geometry.

Raman Spectroscopy Mapping

Raman mapping measurements were performed using a Horiba XploRA confocal Raman system. The system was equipped with a 405 nm UV laser, carefully chosen for its ability to enhance the Raman scattering efficiency while minimizing sample damage. The laser power was strictly controlled to remain under 500 μW to prevent thermal degradation of the sample. This low power, combined with a high-resolution objective (50x long distance), enabled detailed visualization of the sample surface without compromising structural integrity.

The spot size was maintained at 1 μm to ensure high spatial resolution. Raman spectral data were collected using a grating of 1800 grooves per millimeter, which provides finer spectral resolution, crucial for distinguishing subtle features in the spectra. The spectral array was organized into a 50 by 50 grid, totaling 2500 spectra for each mapping session, allowing comprehensive coverage and detailed mapping of the sample area. Each pixel in the spectral image had an accumulation time of 1 second, balancing between signal strength and measurement speed to optimize data quality. All Raman mappings were analyzed using Horiba Labspec 6 imaging and spectroscopy software and the K-means clustering algorithm integrated into the Scikit-learn platform with a previously reported similar method.[35, 36]

Synthesis of S-Bpin

S-Bpin was synthesized according to a previously reported procedure.[27] SEBS (5.00 g, 14.2 mmol of styrene units), B_2Pin_2 (12.7 g, 49.8 mmol, 3.5 equiv), $[IrCl(COD)]_2$ (0.502 g, 1.5 mol % based on the amount of B_2Pin_2), dtbpy (0.401 g, 3 mol % based on the amount of B_2Pin_2), anhydrous THF (50 ml), and a magnetic stirring bar were placed in a 100 ml flame-dried round-bottom flask and purged with argon for 30 min. The reaction flask was sealed under an argon atmosphere and placed in the preheated oil bath at 75 °C. Three separate reactions were carried out in 3 different periods 6, 4, and 2 h, and cooled to room temperature. The solution was diluted with chloroform (50 ml) and precipitated into methanol followed by several washes with methanol. The resulting white color polymer was collected by suction filtration and dried under vacuum at room temperature. The dissolution and precipitation methods were repeated twice to completely remove catalysts and other unreacted small molecules. The S-Bpin formation was confirmed by the ^1H NMR (Figure S1), and FTIR (Figure S4). The degree of functionalization of styrene units of each reaction was calculated from ^1H NMR , based on the relative intensity of the methyl group in the 1,2-butylene unit of the polymer main chain (at 0.84 ppm) with respect to the increased integral ratio of the overlapping SEBS-methylene and boronated ester methyl resonance (at 0.9 to 1.5 ppm).

Synthesis of Tris aminohexadiol (TAHD) Crosslinker

5 g of Tris(2-aminoethyl)amine was added to glysidol (15.2 g) dropwise at 0 °C and run the reaction at room temperature. The reaction mixture formed a gel within 30 min. The amine crosslinker was used directly without any purification. The product was characterized by FTIR and ^{1}H NMR.

Vitrimer Synthesis

S-Bpin (1.00 g) was first dissolved in THF (10 mL). TAHD crosslinker was used as 5 mol% equivalents of grafted boronic esters. 0.008, 0.032, and 0.051g of TAHD crosslinker were dissolved in DMF (1mL) for 10%, 38% and 65% functionalized S-Bpin, respectively. The two solutions were mixed and stirred for 5 minutes at room temperature. The mixture was vacuum-dried at room temperature for one hour and partially cured at 120 °C overnight. The resulting dry sample was cured by hot pressing at 180 °C for 30 minutes.

Preparation of Glass Fiber Composites

The composite was prepared with 30 % polymer loading and 70 % fiber weight. Synthesized S-Bpin (6.30 g) was fully dissolved in THF (30 mL) and mixed with TAHD crosslinker (0.20 g, 5% mol based on the amount of boronic acid functionalization determined by the ^{1}H NMR quantification), dissolved in DMF (1 mL). The solution was mixed for about 1 minute and poured into three layers of plain weave GF cloth (21.0 g) with 6 inches × 5 inches dimensions. The polymer solution was evenly dispersed among the three layers through layer-by-layer deposition. The dried GF composite was obtained after partially curing in a vacuum oven at 120 °C overnight. The dried composite was cured by hot pressing at 180 °C for 45 minutes.

Chemical Recycling of Glass Fiber Composite and S-Bpin

Excess pinacol (5.0 g) was dissolved in THF, and the GF composite (6 inches × 5 inches) was soaked in THF solution at RT overnight, in a sealed container, with continuous stirring at low speed. After the reaction time, the three layers of GFs were carefully removed and rinsed with THF, followed by methanol. The THF and methanol solution used to rinse the GFs was collected and combined with the recycled solution to ensure that all pinacol and S-Bpin crosslinked polymers were retrieved. The GFs were recovered without any physical damage and used to fabricate recycled composite samples. The recovery weight percentage of the retrieved GF was 99% of that of the original GF.

The solution was precipitated into methanol to collect the S-Bpin polymer. The white color solid was collected by suction filtration followed by three washes with methanol to dissolve all the residual pinacol. The recycled S-Bpin was characterized by ^{1}H NMR.

After precipitating pinacol, the filtrate solution was concentrated by rotary evaporation to collect the mixture of TAHD crosslinker and excess pinacol. The TAHD crosslinker was purified and isolated by recrystallizing it twice with water. The TAHD crosslinker recovery was confirmed by FTIR and ^{1}H NMR.

Mechanical Recycling of the Vitrimer

A previously hot-pressed 38% S-Bpin+TAHD film was cut into small pieces and again hot-pressed at 180**°C** for 30 minutes. The resulting film was a defects-free even surface film. The film was cut into dog bone shapes with a dog-bone tensile test piece die-cutting punch press and subjected to tensile test analysis. This procedure was repeated 3 times, and the mechanical properties were tested up to three cycles of each thermally recycled film.

XPS Analysis of Glass Fiber (control) and Recycled Glass Fiber Samples

The unsized Gf sample and chemically recycled GF were mounted directly to the XPS sample holder using metal clips to hold an Al-foil mask over the sample. The Al-foil masks had a small hole (~1 mm diameter) so that the fibers could be directly probed with the x-ray beam. After inserting the sample through a vacuum-pumped load lock into the analysis chamber, a wide energy range survey spectrum was acquired on each sample to determine all elements present. Next, a set of narrow energy range core level spectra were acquired for each identified element.

ACKNOWLEDGEMENTS

The work was supported by the US Department of Energy, Office of Energy Efficiency and Renewable Energy (EERE) Vehicle Technologies Office (VTO). Raman imaging and analysis was supported by the U.S. Department of Energy, Office of Electricity (OE), Energy Storage Division.

References

(1) Witten, E.; Mathes, V. *The Market for Glass Fibre Reinforced Plastics (GRP) in 2020.*; Industrievereinigung Verstärkte Kunststoffe e.V, 2020.

(2) Jensen, J. P.; Skelton, K. Wind turbine blade recycling: Experiences, challenges and possibilities in a circular economy. *Renewable and Sustainable Energy Reviews* **2018**, *97*, 165-176. DOI: https://doi.org/10.1016/j.rser.2018.08.041.

(3) EECI. *Accelerating Wind Turbine Blade Circularity*; WindEurope Brussels, Belgium; Cefic: Brussels, Belgium; EuCIA: Brussels, Belgium, 2018. https://windeurope.org/wp-content/uploads/files/about-wind/reports/WindEurope-Accelerating-wind-turbine-blade-circularity.pdf.

(4) Lukács, T.; Pereszlai, C.; Geier, N. Delamination measurement in glass fibre reinforced polymer (GFRP) composite based on image differencing. *Composites Part B: Engineering* **2023**, *248*, 110381. DOI: https://doi.org/10.1016/j.compositesb.2022.110381.

(5) Kumar Panchagnula, K.; Vamsi Krishna Jasti, N.; Sharma Panchagnula, J. Prediction of drilling induced delamination and circularity deviation in GFRP nanocomposites using deep neural network. *Materials Today: Proceedings* **2022**, *62*, 7118-7123. DOI: https://doi.org/10.1016/j.matpr.2022.02.041.

(6) Liu, Y.; Lu, F.; Yang, L.; Wang, B.; Huang, Y.; Hu, Z. Closed-Loop Recycling of Carbon Fiber-Reinforced Composites Enabled by a Dual-Dynamic Cross-linked Epoxy Network.

ACS Sustainable Chemistry & Engineering **2023**, *11* (4), 1527-1539. DOI: 10.1021/acssuschemeng.2c06322.

(7) Thomason, J. L. Glass fibre sizing: A review. *Composites Part A: Applied Science and Manufacturing* **2019**, *127*, 105619. DOI: https://doi.org/10.1016/j.compositesa.2019.105619.

(8) Cadore-Rodrigues, A. C.; Guilardi, L. F.; Wandscher, V. F.; Pereira, G. K. R.; Valandro, L. F.; Rippe, M. P. Surface treatments of a glass-fiber reinforced composite: Effect on the adhesion to a composite resin. *Journal of Prosthodontic Research* **2020**, *64* (3), 301-306. DOI: https://doi.org/10.1016/j.jpor.2019.09.001.

(9) Ren, D.; Li, K.; Chen, L.; Chen, S.; Han, M.; Xu, M.; Liu, X. Modification on glass fiber surface and their improved properties of fiber-reinforced composites via enhanced interfacial properties. *Composites Part B: Engineering* **2019**, *177*, 107419.

(10) Cromwell, O. R.; Chung, J.; Guan, Z. Malleable and Self-Healing Covalent Polymer Networks through Tunable Dynamic Boronic Ester Bonds. *Journal of the American Chemical Society* **2015**, *137* (20), 6492-6495. DOI: 10.1021/jacs.5b03551.

(11) Wang, S.; Xing, X.; Zhang, X.; Wang, X.; Jing, X. Room-temperature fully recyclable carbon fibre reinforced phenolic composites through dynamic covalent boronic ester bonds. *Journal of Materials Chemistry A* **2018**, *6* (23), 10868-10878, 10.1039/C8TA01801D. DOI: 10.1039/C8TA01801D.

(12) Rahman, M. A.; Bowland, C.; Ge, S.; Acharya, S. R.; Kim, S.; Cooper, V. R.; Chen, X. C.; Irle, S.; Sokolov, A. P.; Savara, A.; et al. Design of tough adhesive from commodity thermoplastics through dynamic crosslinking. *Science Advances* **2021**, *7* (42), eabk2451. DOI: doi:10.1126/sciadv.abk2451.

(13) Taynton, P.; Ni, H.; Zhu, C.; Yu, K.; Loob, S.; Jin, Y.; Qi, H. J.; Zhang, W. Repairable Woven Carbon Fiber Composites with Full Recyclability Enabled by Malleable Polyimine Networks. *Advanced Materials* **2016**, *28* (15), 2904-2909. DOI: https://doi.org/10.1002/adma.201505245.

(14) Spiesschaert, Y.; Guerre, M.; De Baere, I.; Van Paepegem, W.; Winne, J. M.; Du Prez, F. E. Dynamic Curing Agents for Amine-Hardened Epoxy Vitrimers with Short (Re)processing Times. *Macromolecules* **2020**, *53* (7), 2485-2495. DOI: 10.1021/acs.macromol.9b02526.

(15) Yu, L.; Zhu, C.; Sun, X.; Salter, J.; Wu, H.; Jin, Y.; Zhang, W.; Long, R. Rapid Fabrication of Malleable Fiber Reinforced Composites with Vitrimer Powder. *ACS Applied Polymer Materials* **2019**, *1* (9), 2535-2542. DOI: 10.1021/acsapm.9b00641.

(16) Ruiz de Luzuriaga, A.; Martin, R.; Markaide, N.; Rekondo, A.; Cabañero, G.; Rodríguez, J.; Odriozola, I. Epoxy resin with exchangeable disulfide crosslinks to obtain reprocessable, repairable and recyclable fiber-reinforced thermoset composites. *Materials Horizons* **2016**, *3* (3), 241-247, 10.1039/C6MH00029K. DOI: 10.1039/C6MH00029K.

(17) Zhou, Z.; Kim, S.; Bowland, C. C.; Li, B.; Ghezawi, N.; Lara-Curzio, E.; Hassen, A.; Naskar, A. K.; Rahman, M. A.; Saito, T. Unraveling a path for multi-cycle recycling of tailored fiber-reinforced vitrimer composites. *Cell Reports Physical Science* **2022**, *3* (9), 101036. DOI: https://doi.org/10.1016/j.xcrp.2022.101036.

(18) Ying, H.; Zhang, Y.; Cheng, J. Dynamic urea bond for the design of reversible and self-healing polymers. *Nature Communications* **2014**, *5* (1), 3218. DOI: 10.1038/ncomms4218.

(19) Zheng, J.; Png, Z. M.; Ng, S. H.; Tham, G. X.; Ye, E.; Goh, S. S.; Loh, X. J.; Li, Z. Vitrimers: Current research trends and their emerging applications. *Materials Today* **2021**, *51*, 586-625. DOI: https://doi.org/10.1016/j.mattod.2021.07.003.

(20) Paolillo, S.; Bose, R. K.; Santana, M. H.; Grande, A. M. Intrinsic Self-Healing Epoxies in Polymer Matrix Composites (PMCs) for Aerospace Applications. In *Polymers*, 2021; Vol. 13.
(21) Benazzo, F.; Sodano, H. A. Evaluation of Interfacial Shear Strength Healing Efficiency between Dynamic Covalent Bond-Based Epoxy and Functionalized Fiberglass. *ACS Applied Polymer Materials* **2022**, *4* (4), 2925-2934. DOI: 10.1021/acsapm.2c00215.
(22) Long, D. A. Infrared and Raman characteristic group frequencies. Tables and charts George Socrates John Wiley and Sons, Ltd, Chichester, Third Edition, 2001. Price £135. *Journal of Raman Spectroscopy* **2004**, *35* (10), 905-905. DOI: https://doi.org/10.1002/jrs.1238 (acccessed 2024/07/27).
(23) Safi, S.; Zadhoush, A.; Masoomi, M. Effects of chemical surface pretreatment on tensile properties of a single glass fiber and the glass fiber reinforced epoxy composite. *Polymer Composites* **2016**, *37* (1), 91-100. DOI: https://doi.org/10.1002/pc.23158 (acccessed 2024/10/02).
(24) Zhu, J.; Deng, Y.; Chen, P.; Wang, G.; Min, H.; Fang, W. Prediction of Long-Term Tensile Properties of Glass Fiber Reinforced Composites under Acid-Base and Salt Environments. In *Polymers*, 2022; Vol. 14.
(25) Bulut, M.; Alsaadi, M.; Erkliğ, A. A comparative study on the tensile and impact properties of Kevlar, carbon, and S-glass/epoxy composites reinforced with SiC particles. *Materials Research Express* **2018**, *5* (2), 025301. DOI: 10.1088/2053-1591/aaa991.
(26) Nairn, J. A.; Hu, S. Matrix microcracking. *Composite materials series* **1994**, 187-187.
(27) Rahman, M. A.; Karunarathna, M. S.; Bowland, C. C.; Yang, G.; Gainaru, C.; Li, B.; Kim, S.; Chawla, V.; Ghezawi, N.; Meyer, H. M.; et al. Tough and recyclable carbon-fiber composites with exceptional interfacial adhesion via a tailored vitrimer-fiber interface. *Cell Reports Physical Science* **2023**, *4* (12), 101695. DOI: https://doi.org/10.1016/j.xcrp.2023.101695.
(28) Martins, M. L.; Zhao, X.; Demchuk, Z.; Luo, J.; Carden, G. P.; Toleutay, G.; Sokolov, A. P. Viscoelasticity of Polymers with Dynamic Covalent Bonds: Concepts and Misconceptions. *Macromolecules* **2023**, *56* (21), 8688-8696. DOI: 10.1021/acs.macromol.3c01545.
(29) Ferry, J. D. *Viscoelastic properties of polymers*; John Wiley & Sons, 1980.
(30) Soman, B.; Schweizer, K. S.; Evans, C. M. Fragile Glass Formation and Non-Arrhenius Upturns in Ethylene Vitrimers Revealed by Dielectric Spectroscopy. *Macromolecules* **2023**, *56* (1), 166-176. DOI: 10.1021/acs.macromol.2c01657.
(31) Ge, S.; Tsao, Y.-H.; Evans, C. M. Polymer architecture dictates multiple relaxation processes in soft networks with two orthogonal dynamic bonds. *Nature Communications* **2023**, *14* (1), 7244. DOI: 10.1038/s41467-023-43073-w.
(32) Ni, J.; Min, J.; Wan, H.; Lin, J.; Wang, S.; Wan, Q. Effect of adhesive type on mechanical properties of galvanized steel/SMC adhesive-bonded joints. *International Journal of Adhesion and Adhesives* **2020**, *97*, 102482. DOI: https://doi.org/10.1016/j.ijadhadh.2019.102482.
(33) Banea, M. D.; da Silva, L. F. M.; Carbas, R.; Campilho, R. D. S. G. Effect of material on the mechanical behaviour of adhesive joints for the automotive industry. *Journal of adhesion science and Technology* **2017**, *31* (6), 663-676.
(34) Prolongo, S. G.; del Rosario, G.; Ureña, A. Comparative study on the adhesive properties of different epoxy resins. *International Journal of Adhesion and Adhesives* **2006**, *26* (3), 125-132. DOI: https://doi.org/10.1016/j.ijadhadh.2005.02.004.

(35) Pedregosa, F.; Varoquaux, G.; Gramfort, A.; Michel, V.; Thirion, B.; Grisel, O.; Blondel, M.; Prettenhofer, P.; Weiss, R.; Dubourg, V. Scikit-learn: Machine learning in Python. *the Journal of machine Learning research* **2011**, *12*, 2825-2830.
(36) Yang, G.; Tao, R.; Jafta, C. J.; Shen, C.; Zhao, S.; He, L.; Belharouak, I.; Nanda, J. Investigating Multiscale Spatial Distribution of Sulfur in a CNT Scaffold and Its Impact on Li–S Cell Performance. *The Journal of Physical Chemistry C* **2021**, *125* (24), 13146-13157. DOI: 10.1021/acs.jpcc.1c02288.

Data Availability

The data supporting this article have been included as part of the SI.